Structure of the Cesium Salt of an Ethylene-Methacrylic Acid Copolymer from Its Radial Distribution Function

J. Kao, R. S. Stein, W. J. MacKnight,* W. P. Taggart, and G. S. Cargill, III

Department of Chemistry and Polymer Science and Engineering, University of Massachusetts, Amherst, Massachusetts 01002. *Received July 16, 1973*

ABSTRACT: A poly(ethylene-*co*-methacrylic acid) polymer containing 3.8 mol % methacrylic acid and it's 64% neutralized cesium salt were subjected to a small- and wide-angle X-ray scattering study. The radial distribution functions (RDF's) were obtained by carrying out the Fourier transforms of the angular dependences of the scattered X-ray intensities. The RDF of the acid form was subtracted from the RDF of the salt form to approximately cancel the light atom contributions leaving only cesium atom contributions. The results of these analyses indicate that electron density fluctuations having spatial extents of the order of 20 Å are present in the salt but absent in the acid copolymer. One model consistent with these results is an ionic cluster model in which the metal atoms tend to segregate in regions of 20-Å diameter. An attempt was made to fit a hard sphere cluster model to the experimental RDF but this was found to be inadequate to account for the data.

The properties of synthetic polymers containing salt groups have been extensively investigated in recent years. Much of this work is well summarized in the review of Otocka.[1] An important class of these polymers is the ethylene-carboxylic acid copolymers which have been either partially or wholly neutralized with a cation such as sodium. On neutralization of the carboxylic acid side groups it is found that properties such as optical clarity, tensile strength, impact resistance, and melt viscosity are dramatically enhanced.[2] At least two structural models have been put forward to account for these phenomena. In the first, a three-phase model is envisaged, consisting of a polyethylene crystal phase, an amorphous hydrocarbon phase, and a phase consisting of microphase separated clusters of salt groups, 100 Å or less in size.[2-5] The other model postulates a uniform distribution of salt groups throughout the amorphous phase.[6,7] In this latter model it is assumed that the salt groups form dimers but do not cluster to any significant extent.

Wide-angle X-ray diffraction studies have been carried out on these polymers and some typical results are shown in Figure 1.[3] It is immediately obvious that a fundamental change occurs in going from the acid to the salt form. In particular, a new peak occurs in the salt form at $2\theta \approx 4°$. The 110 and 200 diffraction peaks characteristic of polyethylene-like crystallinity, as well as the amorphous halo are common to both forms. This new peak occurs in all neutralized polymers regardless of the nature of the cation, is sensitive to the concentration of cation, disappears when the material is saturated with water, and persists to temperatures in excess of 200°.[3] It origin has been ascribed to diffraction arising from ordered structures existing within ionic domains.[3] More recently, two alternate explanations have been put forward. The first proposes that the salt groups form small aggregates at a characteristic distance apart and that this distance corresponds to the Bragg spacing of the peak.[8a] The second interpretation envisions the peak to arise from a characteristic spacing between ionic clusters and matrix ions which are attracted to these clusters by an electrostatic potential present as a result of a tendency for charge imbalance to exist in the clusters because of the coordination of the metal ions with several anions.[8b] Whatever the true origin of this peak, it is clear that it is connected with the presence of salt groups and arises from some structural feature occurring as a consequence of the neutralization of the acid copolymer.

An approach to the problem of determining the distribution of salt groups in these polymers is through the radial distribution function (RDF) which may be obtained as the Fourier transform of the angular dependence of the scattered X-ray intensities. The procedure is to take the difference between the RDF's of the acid and cesium salt forms of the same copolymer. This has the effect of cancelling contributions from light atoms leaving only peaks arising from the cesium atoms. Such a procedure has been carried out by Roe[9] on an ethylene-acrylic acid copolymer containing 12.6 wt % acrylic (5.35 mol %) acid and its 78% neutralized cesium salt. Roe concluded from this study that there was no evidence for the formation of clusters of ionic groups of around 15 Å or smaller in size but that there was strong evidence for dimer formation. The results could not rule out the possible formation of large clusters but these were held unlikely on thermodynamic grounds.[10]

RDF's derived from experimental X-ray scattering data must be interpreted with caution since they are susceptible to a number of inaccuracies arising from various sources. These include absorption corrections, normalization, termination of the experimental data at a finite scattering vector,[11] and neglected contributions from small-angle X-ray scattering.[12] Roe did not have careful measurements of scattered intensity below $s = 0.6$ Å^{-1}, *i.e.*, in the small-angle region containing the ionic peak shown in Figures 1 and 3 and discussed above. His cesium neutralized ethylene-acrylic acid copolymer is chemically similar to systems in which such ionic peaks have been observed. Indeed, his two data points for $s < 0.6$ Å^{-1} suggest the presence of a small-angle peak for his neutralized specimen. Because Roe largely ignored the small-angle region in which the ionic peak is expected and because this peak may significantly affect the RDF of the salt form and

(1) E. P. Otocka, *J. Macromol. Sci., Rev. Macromol. Chem.*, **5**, 275 (1971).
(2) R. Longworth and D. J. Vaughan, *Nature (London)*, **218**, 85 (1968).
(3) F. C. Wilson, R. Longworth, and D. J. Vaughan, *Polym. Prepr., Amer. Chem. Soc., Div. Polym. Chem.*, **9**, 505 (1968).
(4) H. A. Davis, R. Longworth, and D. J. Vaughan, *Polym. Prepr., Amer. Chem. Soc., Div. Polym. Chem.*, **9**, 515 (1968).
(5) W. J. MacKnight in "Colloidal and Morphological Behavior of Block and Graft Copolymers," G. Molau, Ed., Plenum Press, New York, N. Y., 1971, p 131.
(6) E. P. Otocka and T. K. Kwei, *Macromolecules*, **1**, 401 (1968).
(7) E. P. Otocka and D. D. Davis, *Macromolecules*, **2**, 437 (1969).
(8) (a) C. L. Marx, D. F. Caufield, and S. L. Cooper, *Polym. Prepr., Amer. Chem. Soc., Div. Polym. Chem.*, **14**, 2 (1973); *Macromolecules*, **6**, 344 (1973). (b) W. J. MacKnight, W. P. Taggart, and R. S. Stein, *J. Polym. Sci., Part C*, in press.
(9) R. J. Roe, *J. Phys. Chem.*, **76**, 1311 (1972).
(10) A. Eisenberg, *Macromolecules*, **3**, 147 (1970).
(11) R. Kaplow, S. L. Strong, and B. L. Auerback, *Phys. Rev.*, **138**, A1336 (1965).
(12) G. S. Cargill III, *J. Appl. Crystallogr.*, **4**, 277 (1971).

Table I

	f_e, Coherent Scattering Factor				$(I_{inc})_i$,[a] Incoherent Scattering Intensity Factor				
sin θ/λ	C[b]	H[c]	O[b]	Cs[b]	C[e]	H[f]	O[e]	Cs[d]	f_e^2
0.00	6.00	1.000	8.00	54.00	0.000	0.000	0.000	0.000	1.000
0.05	5.76	0.947	7.81	53.14	0.363	0.103	0.271	1.793	0.893
0.10	5.14	0.811	7.28	50.83	1.221	0.343	0.977	4.320	0.657
0.15	4.38	0.641	6.54	47.68	2.159	0.589	1.885	7.623	0.411
0.20	3.66	0.481	5.73	44.31	2.925	0.769	2.799	9.615	0.231
0.30	2.60	0.251	4.24	38.26	3.829	0.937	4.293	14.217	0.063
0.40	2.02	0.130	3.16	33.53	4.240	0.983	5.257	17.753	0.017
0.50	1.72	0.071	2.46	29.66	4.488	0.995	5.828	20.612	0.0050
0.60	1.55	0.040	2.02	26.35	4.690	0.998	6.175	23.228	0.0016
0.70	1.44	0.024	1.76	23.56	4.876	0.999	6.411	25.694	0.0006
0.80	1.33	0.015	1.59	21.28	5.050	1.000	6.596	28.981	
0.90	1.23	0.010	1.48	19.47	5.270	1.000	6.755	30.064	
1.00	1.13	0.007	1.39	18.02	5.347	1.000	6.901	31.914	
1.50	0.66	0.0015	1.01	12.96	5.780	1.000	7.462	38.232	

[a] These values are the total theoretical Compton scattering intensities. The actual values for the corrections are less than this due to diffracted beam monochromater of 0.04-Å band pass. The detailed calculations are given by W. Ruland, *Brit. J. Appl. Phys.*, **15**, 1301 (1964). [b] D. T. Cromer and J. T. Waber, *Acta Crystallogr.*, **18**, 104 (1965). [c] International Tables for X-ray Crystallography, Vol. 3. [d] D. T. Cromer and J. B. Mann, *J. Chem. Phys.*, **47**, 1892 (1967). [e] D. T. Cromer, *J. Chem. Phys.*, **50**, 4857 (1969). [f] By using the relation, $I_{inc} = z - \Sigma_n f_{nn}^2$ and $I_{inc} = 1 = f_H^2$.

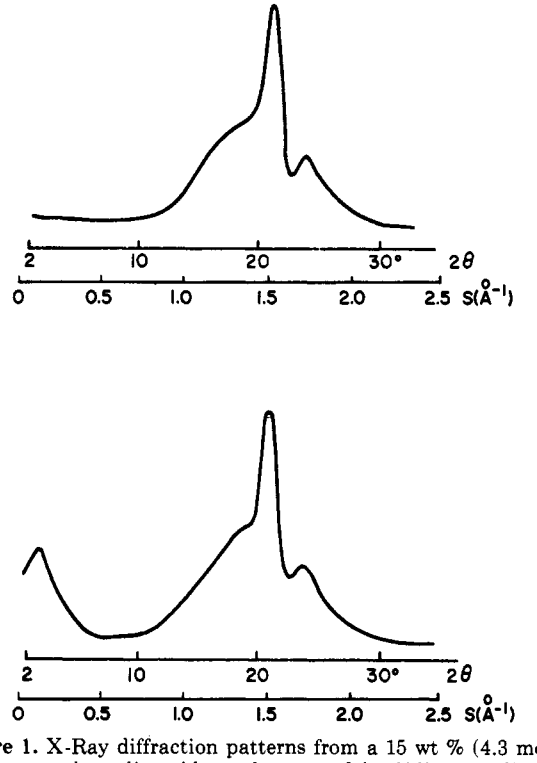

Figure 1. X-Ray diffraction patterns from a 15 wt % (4.3 mol %) ethylene-methacrylic acid copolymer and its 95% neutralized sodium salt (3).

thereby conclusions based on the RDF about the distribution of salt groups in the copolymer, we have calculated the RDF's for an ethylene-methacrylic acid copolymer and its cesium salt following Roe's method but including the "ionic" peak. One model consistent with the results is the presence of salt clusters or domains containing approximately 50 cesium atoms/cluster in the copolymer investigated. A number of studies exist indicating that there is little difference in properties between acrylic acid copolymers and methacrylic acid copolymers although minor differences cannot be ruled out.[1-6]

Experimental Section

A. Sample Preparation. The starting copolymer is identical with that used in previous studies from these laboratories[5] and contains 3.8 mol % methacrylic acid. The cesium salt was prepared by a method already described[13] and the cesium content, determined by elemental analysis, corresponded to 64% neutralization of the acid groups. The salt and the acid samples were both annealed at 90° for 24 hr.

B. Wide-Angle X-Ray Scattering Data (WAXS). WAXS data from $2\theta = 2.0°$ to 115° were obtained by the symmetric transmission method using an X-ray diffractometer manufactured by General Electric Co. Mo Kα radiation was used and a LiF crystal in the diffracted beam served as a monochromator. The slit openings were 1.0° for the primary beam and 0.3° for the scattered beam. At least 5000 total counts were taken for all measurements to yield a statistical counting error of less than 1%. Step sizes were 0.25° from 2.0 to 25.0°, 0.5° from 25.0 to 55.0° and 1.0° from 55.0 to 115°, both for the samples and for background scattering determinations. Two runs were made for each sample and the data were smoothed before any corrections were made.

Correction for the background scattering was made to the measured intensity, I_{meas}, to yield the corrected intensity, I_{cor}. Assuming that the background scattering is proportional to the intensity of the main beam only, the main beam and the background scattering are both attenuated due to the presence of the sample by the factor $e^{-\mu t/\cos\theta}$, where μ is the absorption coefficient of the sample. I_{cor} then follows from

$$I_{cor} = (I_{meas} - I_b e^{-\mu t/\cos\theta})(A_s/P) \quad (1)$$

where I_b is the background scattering, A_s is the absorption correction factor for symmetric transmission geometry, and P is the polarization factor.

$$A_s = e^{-\mu t(1-\sec\theta)}/\sec\theta \quad (2)$$

$$P = (1 + \cos^2 2\alpha \cos^2 2\theta)/(1 + \cos^2 2\alpha) \quad (3)$$

In eq 3, α is the Bragg angle for the reflecting plane of the monochromator. Here, $\alpha = 22.48°$.

C. Small-Angle X-Ray Scattering Data (SAXS). SAXS data were collected using a Rigaku Denki goniometer in conjunction with Cu Kα radiation in the angular range from $2\theta = 0.1°$ to $2\theta = 7.5°$. The main beam is defined between the sample and focal point, a distance of 362 mm, by two 0.1 × 10.0 mm slits and a scattering slit. Between the sample and detector, a distance of 267 mm apart, there are a receiving slit 0.05 × 15 mm, a scattering slit, and the whole is enclosed in a vacuum chamber to eliminate air scattering. Monochromatization is achieved using a nickel filter in conjunction with a pulse height analyzer. Data taken using a minimum of 5000 counts for each measurement were smoothed and corrected for polarization, absorption, background scattering, and slit height collimation. The slit height collimation correction was performed according to the method of Schmidt.[14]

(13) W. J. MacKnight, L. W. McKenna, B. E. Read, and R. S. Stein, *J. Phys. Chem.*, **72**, 1122 (1968).
(14) P. W. Schmidt, *Acta Crystallogr.*, **19**, 938 (1965).

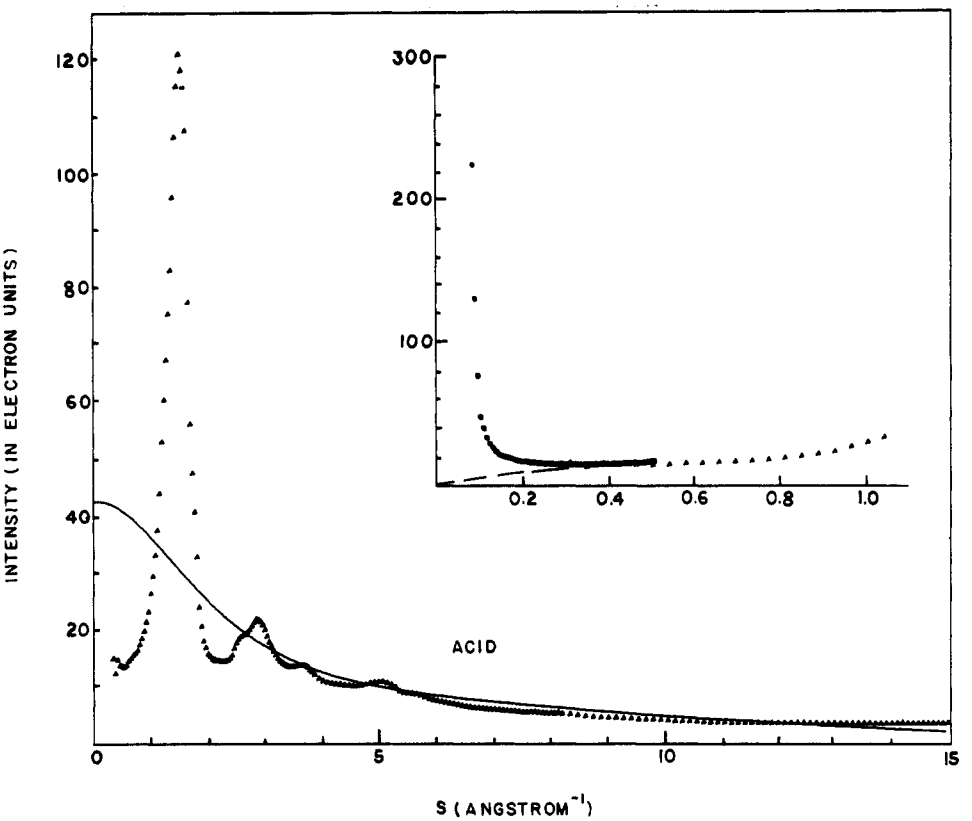

Figure 2. Observed X-Ray scattering intensity of the acid form of the copolymer corrected for background, absorption, and polarization against $s = 4\pi \sin\theta/\lambda$: Δ, wide-angle data; θ, small-angle data. The solid curve represents the independent scattering which consists of coherent scattering and Compton scattering. The dotted lines are used for calculating the interference intensity shown in Figure 4.

Results and Discussion

We define a structural unit as that having an average composition of a unit containing one backbone carbon atom and let n_i represent the number of i-type atoms in a structural unit. The values of the n_i's are: C(1.038), H(2.038), O(0.0381) for the acid, and C(1.038), H(2.026), O(0.0381), and Cs(0.012) for the salt.

The intensity I (in electron units) of X-rays scattered by an amorphous medium without prefered orientation is related to the radial distribution function (RDF) by eq 4,

$$I(s) = N\sum_{i=1}^{m} n_i f_i^2 + N\sum_{i=1}^{m} n_i (I_{inc})_i + \left(\frac{4\pi N}{s}\right)\int_0^\infty r \sin sr \sum_{i=1}^{m}\sum_{j=1}^{m} n_i f_i f_j [\rho_{ij}(r) - \rho_{ij}(\infty)]dr \quad (4)$$

where N = the total number of structural units contributing to the scattered intensity; n_i = number of i-type atoms in a structural unit; f_i = the atomic scattering factor of i-type atoms; $(I_{inc})_i$ = the Compton scattering factor of I-type atoms; m = the number of different kinds of atoms present in the structural unit, here, $m = 3$ for the acid and $m = 4$ for the salt; $s = 4\pi \sin\theta/\lambda$, where λ is the wavelength of the radiation; 2θ is the scattering angle; $\rho_{ij}(r)$ = the number of j-type atoms per unit volume at a distance r from a given i-type atom; $\rho_{ij}(\infty)$ = the average number of j-type atoms per unit volume.

We define an average scattering factor per electron

$$\langle f_e \rangle = \left(\sum_{i=1}^{m} n_i f_i\right) / \sum_{i=1}^{m} n_i z_i \quad (5)$$

We next represent the scattering factor in terms of $\langle f_e \rangle$ by the relation

$$f_i = K_i \langle f_e \rangle \quad (6)$$

The effective electron numbers K_i defined by eq 6 will be approximately equal to the atomic numbers z_i. For each kind of atom the effective number K_i will vary somewhat with s and the approximation which we are making involves using an average value and treating K_i as a constant for each kind of atom. Note that the average scattering factor $\langle f_e \rangle$ decreases with s comparatively less rapidly than the one used by Roe. However, since both approximations gave similar results for the RDF function, we shall only treat our data according to this relation.

Combining eq 4, 5, and 6, we obtain

$$i(s) = \left[\frac{I(s)}{N} - \sum_{i=1}^{m} n_i f_i^2 - \sum_{i=1}^{m} n_i (I_{inc})_i\right] / \langle f_e \rangle^2 \quad (7)$$

$$si(s) = 4\pi \int_0^\infty r \sin sr \sum_{i=1}^{m}\sum_{j=1}^{m} n_i n_j K_i K_j [\rho_{ij}(r) - \rho_{ij}(\infty)]dr \quad (8)$$

The interference intensity defined in eq 8 contains all available information about the arrangement of the atoms in space.

By application of the Fourier inverse theorem to eq 8, one obtains

$$4\pi r[D(r) - D_0] = (2/\pi)\int_0^\infty si(s) \sin srds \quad (9)$$

where

$$D(r) = \sum_{i=1}^{m}\sum_{j=1}^{m} n_i K_i K_j \rho_{ij}(r) \quad (10)$$

$D(r)$ represents the superposition of the RDF's for each kind of atom and $D_0 = D_{ij}(\infty)$.

Figure 2 is a plot of $I(s)$ for the acid copolymer, including corrections for background, absorption, and polarization. The small-angle data also include a slit length colli-

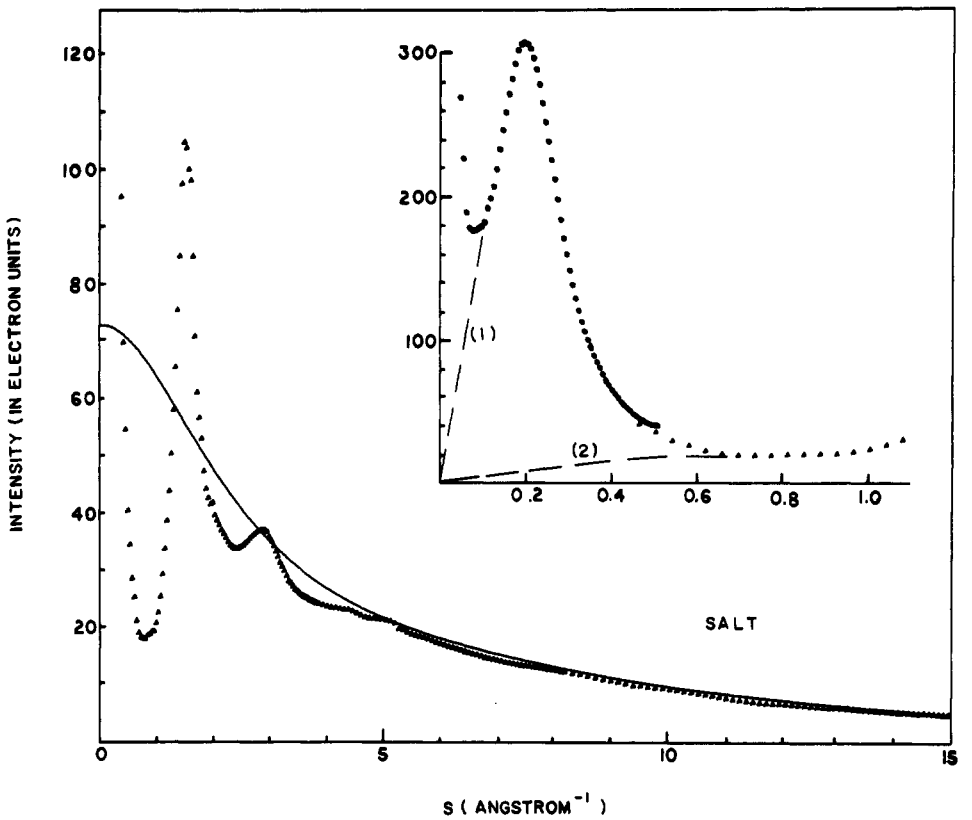

Figure 3. Same plot as Figure 2 but for the salt form. The values on dotted line (1) and dotted line (2) are used for the interference intensities shown in Figure 4. We specify these two sets of data as Salt (1) and Salt (2), respectively.

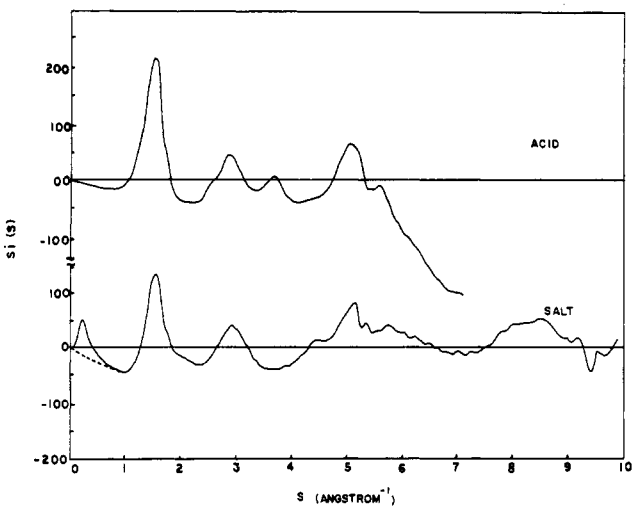

Figure 4. The interference intensity $i(s)$ multiplied by s against s. The top figure is for the acid, the bottom one is for the Salt (1), and the bottom one with the dotted line for small values of s is for Salt (2).

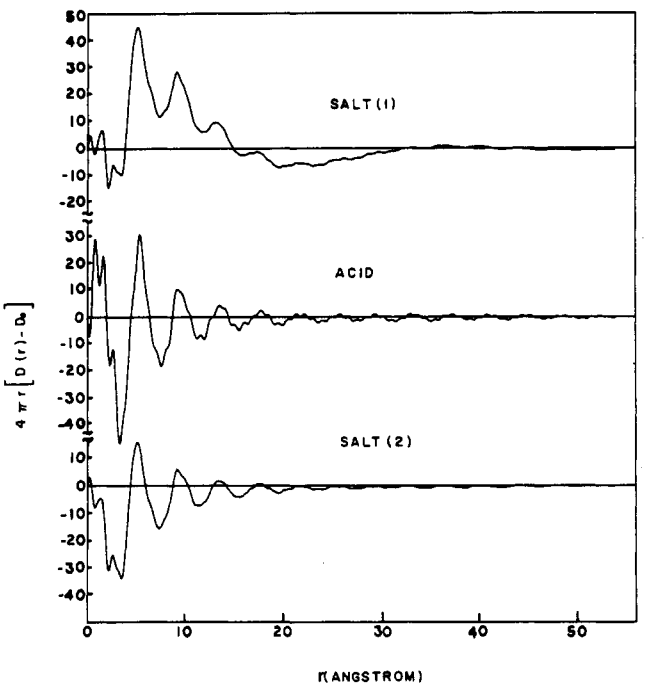

Figure 5. Results from the Fourier transformation of $si(s)$ shown in Figure 4. Salt (1) is the result with the small-angle peak (s = 0.195 Å^{-1}) Salt (2) is the result without the small-angle peak.

mation correction. The independent scattering contribution to $I(s)$ is represented by the solid line in Figure 2 and consists of the coherent scattering and Compton scattering. The coherent scattering factors and Compton scattering factors used to construct the solid curve in Figure 2 are collected in Table I. The normalization of the experimental values of $I(s)$ to an absolute scale in electron units was accomplished by matching the observed intensity at high s values to the independent scattering intensity. Figure 3 is a similar plot to Figure 2, except for the cesium salt rather than the acid. From the data plotted in Figures 2 and 3 and eq 7, we obtain $si(s)$, which is plotted against s in Figure 4 for both the acid and salt forms of the copolymer. The plot in Figure 4 for the salt is qualitatively similar to that of Roe if the dotted portion of the curve is used at small values of s but the intensities are considerably larger. This is probably due in part to the fact that our samples were annealed. This plot is designated Salt (2). As already pointed out, this neglects the "ionomer" peak present in the salt sample. The solid curve includes this peak at small s values and is designated Salt (1).

Any inaccuracies in the corrected scattering intensity

Table II
Maxima in Radial Distribution Functions (s, Å^{-1})

	Acid	Salt (1)	Salt (2)
r_1	0.71 ± 0.05	0.22	0.22
r_2	1.56	1.42	1.49
r_3	2.47	2.55	2.60
r_4	5.28	5.08	5.08
r_5	9.14	9.15	9.23

$I(s)$ would be greatly enhanced at large s by multiplication by s and $1/\langle f_e\rangle^2$. Therefore the plots in Figure 4 are arbitrarily terminated to avoid obvious errors at large s values.

At very small s values, below about s = 0.1 Å^{-1}, both acid and salt scatter strongly. This scattering arises largely from the crystal lamellae in both cases. In the salt, additional contributions are present from the ionic portions. Our neglecting this very small angle scattering will introduce some long-wavelength (>50 Å) errors into the final RDF. The Fourier transform of $si(s)$, shown in Figure 5, was evaluated on a CDC 3600 computer using the "Fast Discrete Fourier Transformation" subroutine of Starshak and Larsen.[15]

We used 1024 data points from s = 0 to s = 29.8 Å^{-1} at equal intervals of Δs = 0.0291Å^{-1} in which zeros were used for those data points not obtainable from experiment.

The integration of eq 9 should, of course, be carried out from 0 to ∞ but data over the complete range are not available as already discussed. Truncation of the integration at finite values of s_{max} usually leads to the introduction of false peaks at small atomic distance r into the RDF. This difficulty is usually overcome by multiplying $si(s)$ by a convergence function. We have used two such functions: (1) a Gaussian function, $e^{-\alpha s^2}$ with α = 0.01, and (2) a modified sine function equal to 1 from s = 0 to $(3/4)s_{max}$ and decreasing to zero sinusoidally from $(3/4)s_{max}$ to s_{max}. The results are similar for both except that the sine function results in somewhat narrower peaks. The RDF's in Figure 5 are based on a Gaussian convergence factor. These RDF's contain the essential contributions of this work. The important point is that the curves are shaped differently for Salt (1) which includes the "ionomer" peak and Salt (2) which omits this peak. It is thus apparent that structural conclusions drawn from the RDF of Salt (2) may be incorrect.

The remainder of the analysis follows the method of Roe and is summarized below.[9]

The maxima in the RDF's are collected in Table II. The r_1 peaks for both the acid and salt are false peaks arising from the data treatment. This is shown by the fact that the positions of the r_1 peaks vary with the choice of s_{max}. Possibly they arise from a combination of truncation errors and improper choice of normalization constant. r_2 and r_3 represent distances between carbon—carbon pairs which are nearest and next-nearest neighbors in the same chain. Presumably r_4 and r_5 have their origins in interchain distances between carbon—carbon pairs.

Subtracting the RDF of the salt from that of the acid results in

$$\Delta D(r) = D^S(r) - D^A(r) \approx n_1 K_1 \left[K_i \rho_{11}(r) + 2\sum_{j=2}^{4} K_j \rho_{1j}(r) \right] \quad (11)$$

where $D^S(r)$ is the RDF of the salt, $D^A(r)$ is the RDF of the acid, subscript 1 represents the Cs atom, and j represents the other atoms. Equation 12 results from the assumption that the spatial arrangements of the C, H, and O atoms remain the same when H is replaced by Cs. The first term of eq 12 is important only when the cesium atoms tend to cluster and should contribute to $\Delta D(r)$ at values of r greater than 4 Å. This is exactly the situation shown in the top curve of Figure 6. Neglect of the small-angle "ionomer" peak leads to the second curve in Figure 6 which is essentially identical with Roe's results for $\Delta D(r)$ and would tend to rule out the presence of clusters. The contribution of the ionomer peak shows up very markedly in the bottom curve of Figure 6 which results from the subtraction of the RDF of Salt (2) from that of Salt (1).

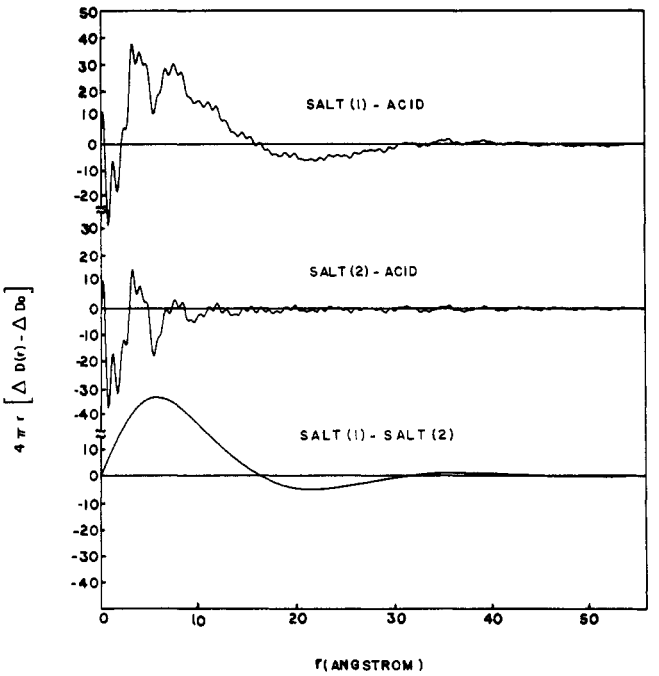

Figure 6. The differences of the three curves shown in Figure 5. The top curve is the plot of $4\pi r[\Delta D(r) - \Delta D_0]$ *vs.* s where the small-angle peak (s = 0.195 Å^{-1}) is included in the data. The middle curve is a similar plot to the top one without the small-angle peak in the salt data. The bottom one is the contribution to the radial distribution function of the salt from the small-angle peak alone.

Following Roe's analysis, his hard sphere model may be used to calculate a theoretical $[\Delta D(r) - \Delta D_0]$ to compare with the experimental $[\Delta D(r) - \Delta D_0]$ presented as the top curve in Figure 6. Before proceeding, it is worth noting some features of the experimental $[\Delta D(r) - \Delta D_0]$. First, attention is drawn to the two peaks in the 3- to 9-Å region. The presence of these peaks may indicate structure within clusters. Such structure cannot be predicted from the hard sphere model employed here. A more refined model is currently under development. Secondly, the experimental $[\Delta D(r) - \Delta D_0]$ becomes negative at distances greater than 16 Å. This feature indicates the absence of pairs of heavy particles separated by a distance larger than the cluster diameter. Finally, the experimental $[\Delta D(r) - \Delta D_0]$ becomes positive again at distances larger than 30 Å and there is the suggestion of a shallow, broad peak centered around 35 Å. It is obviously not possible to be certain about the position of this peak from the available data but its presence is to be expected as arising from contributions to $[\Delta D(r) - \Delta D_0]$ from heavy particle pairs belonging to different clusters. The peak maximum is then to be identified with the average intercluster distance.

In order to be quite clear about the model, the essential

(15) A. J. Starshak and R. D. Larsen, *Phys. Chem. Liq.*, 2, 45 (1970).

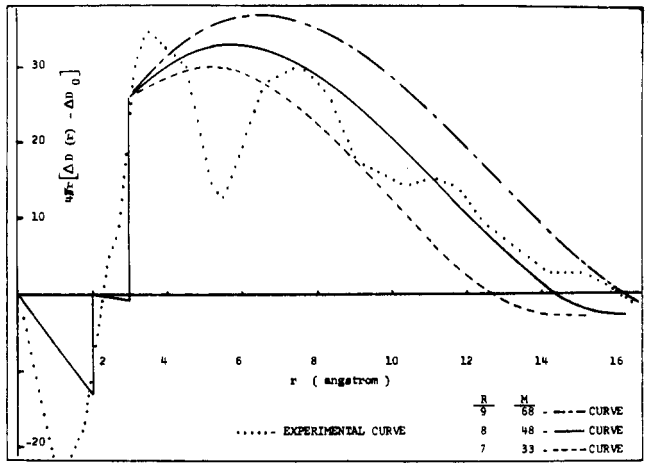

Figure 7. Theoretical values of $4\pi r[\Delta D(r) - \Delta D_0]$ compared to experimental results for R = 7, 8, and 9 and various values of M. R is the radius of the cluster and M is the number of cesium atoms per cluster.

equations are reproduced here from Roe's work.

$$\Delta D(r) = n_H Z_H^2 \rho_{HH}(r) + 2n_H Z_H Z_L \rho_{HL}(r) \quad (12)$$

Quantities in this equation are similar to those employed earlier. For example, $\rho_{HL}(r)$ is the probability of finding a light particle in a unit volume separated by a distance r from a heavy particle.

$$\begin{aligned} \rho_{HL}(r) &= 0 \qquad r \leq r_{HL}^0 \\ \rho_{HL}(r) &= \rho_L^0 \qquad r > r_{HL}^0 \end{aligned} \quad (13)$$

r_{HL}^0 is the limiting approach distance of a heavy and light particle.

$$\begin{aligned} \rho_{HH}(r) &= 0 \qquad r \leq r_{HH}^0 \\ \rho_{HH}(r) &= [(M-1)/v\beta]\alpha(r/R) \qquad r_{HH}^0 < r < 2R \end{aligned} \quad (14)$$

Here, M is the number of heavy particles in the cluster, $v\beta$ is the volume inside the cluster available to the $(M - 1)$ heavy particles other than the one being considered, and $\alpha(r/R)$ is the probability that the end of a vector of length r starting from any point inside the cluster remains within the cluster. The parameters α and β are of well-known mathematical form for the hard sphere model and are given explicitly by Roe.

The model as set forth above does not consider any intercluster contributions and must therefore apply to the experimental results only at distances of less than 30 Å.

In our calculations, the values of r_{HH}^0 and r_{HL}^0 were assumed to be 3.0 and 2.0 Å, respectively, and (V/N), the volume of a structural unit was taken to be 25 Å.[3] These values were selected to give the best hard sphere fit to the experimental results. In addition, the packing density of spheres within the clusters was assumed to be the same for all values of R and M. Thus the calculations converge to essentially the same values of $4\pi r[\Delta D(r) - \Delta D_0]$ at 3 Å which is different from Roe's calculations. The results are shown in Figure 7 for three different values of R and M. Values of R, the radius of spherical domain in which heavy particles are concentrated, were arrived at by taking R to be approximately ½ the distance at which the experimental curve goes to 0. Values of M were obtained from the following consideration. According to Eisenberg, the maximum number of ion pairs which can directly associate is 8 and this is based upon steric considerations. If we assume a cluster to be made up of these structural units, called multiplets by Eisenberg, then M will be the total number of ion pairs determined by how many multiplets can be packed into a cluster. Assuming a multiplet consists of an ionic "core" of radius 3 Å and a hydrocarbon "skin" of radius 1 Å and that these multiplets are spherically close packed in the cluster, values of M are derived for each R as shown in Figure 7.

It can be seen that all of the calculated curves lie below the first experimental peak maximum and that none of them reproduce the experimental peaks and valleys. The curve with R = 9 and M = 68 perhaps gives the best fit. On the assumptions stated, this would correspond to 8–9 multiplets/cluster.

Although the hard sphere model is inadequate to account for the data, the features of the experimental $[\Delta D(r) - \Delta D_0]$ curve indicate that electron density fluctuations having spatial extents on the order of 20 Å are present in the salt but absent in the acid copolymer. One model consistent with these results is that of ionic clusters. It has already been noted that there are some differences between our sample and that of Roe, both with regard to composition and thermal treatment. We do not feel that these differences would affect ionic clustering tendencies very much. The different RDF obtained by us from that of Roe primarily results from the more accurate inclusion of low-angle data in our case.

Acknowledgment. We are grateful to the National Science Foundation for partial support of this research under Grant GH 33129X. Acknowledgment is made to the Donors of the Petroleum Research Fund, administered by the American Chemical Society, for the partial support of this research.